Acoustic propagation in gassy intertidal marine sediments: an experimental study

Timothy G. Leighton[1], Hakan Dogan[1], Paul Fox[1], Agni Mantouka[1], Angus I. Best[2], Gary B. R. Robb[2] and Paul R. White[1]

[1] *Institute of Sound and Vibration Research, University of Southampton, SO17 1BJ, Southampton, UK*

[2] *National Oceanography Centre, European Way, Southampton, SO14 3ZH, UK*

Abstract

The need to predict acoustic propagation through marine sediments that contain gas bubbles has become increasingly important for civil engineering and climate studies. There are relatively few *in situ* acoustic wave propagation studies of muddy intertidal sediments, in which bubbles of biogenic gas (generally methane, a potent greenhouse gas) are commonly found. We used a single experimental rig to conduct two *in situ* intertidal acoustical experiments to improve understanding of acoustic remote sensing of gassy sediments, eventually including gas bubble size distributions. In the first experiment, we measured sediment sound speed and attenuation between four aligned hydrophones for a quasi-plane wave propagating along the array. The second experiment involved a focused insonified sediment volume created by two transducers emitting coincident sound beams at different frequencies that generated bubble-mediated acoustic signals at combination frequencies. The results from sediment core analyses, and comparison of *in situ* acoustic velocity and attenuation values with those of water-saturated sediments, together provide ample evidence for the presence of *in situ* gas bubbles in the insonified volumes of sediments. These datasets are suitable for linear and non-linear inversion studies that estimate *in situ* greenhouse gas bubble populations, needed for future acoustical remote sensing applications.

Keywords: acoustic propagation, sediments, shallow gas, transmission experiments, combination frequency

I. INTRODUCTION

This study measures the populations of gas bubbles in intertidal marine sediments using split sediment cores, and measures the effect these bubbles have on acoustic sound speed and attenuation, and the formation of combination-frequencies. This work parallels a study to develop propagation models for such environments [1-3].

In addition to being important in its own right (see Conclusions), the intertidal zone can provide an accessible, though potentially rapidly-varying, site to test novel sensors, for later deployment in deep-water sites (to study geohazard assessment [4], global climate change [5], seafloor surveying [6-8], the construction of offshore structures [9], and the detection of leakages from carbon capture and storage facilities [10-13]). *In situ* gas generation may have pronounced environmental consequences. In geological environments such as deep-water basins, continental margins and polar slopes, an increase in temperature or a decrease in pressure may cause hydrate to dissociate and release methane gas, weakening the shear strength of the sediment [14]. Furthermore, part of this methane can find various pathways to escape through natural gas seeps and be released into the atmosphere, thereby presenting a possible issue for global climate change [6, 15]. Judd *et al.* [14] estimate that 1.2 to 3.6 % of global methane emissions into the atmosphere arise from continental shelf sediments.

A variety of high-resolution, underwater acoustic systems can map gassy areas [10, 16]. Consequently, the classification of the gas accumulation based on various seismic features is well developed, involving gas plumes, curtains, acoustic turbidity, blanking and chimneys [5]. This classification is motivated by the excessive reverberation and backscatter of sound from the seabed, which is a consequence of the gas-bearing areas that hinder acoustic penetration [17], although sound speed perturbations near such blanking can yield estimates of gas content [18, 19]. For this reason, these acoustic surveys are the most frequently used evidence to infer the presence of gas, which is abundant in the near surface of marine sediments [20]. Despite the advances in remote sensing, detection, mapping of gas and the extensive results on the void fraction of gas (see Table 1 of [18]), the size distribution of gas bubbles is not broadly reported [18].

At present, the most common way to measure bubble distributions in sediments is through X-ray CT scanning of pressurized cores [21-25]. Such methods are limited, owing to the difficulty of collecting pressurized cores, and the inability to relate directly to remote (acoustic or any other type of) measurements. Geochemical methods [26, 27], likewise, are not very practical and require *in situ* coring operations. Moreover, they are labor intensive and do not provide a generalized method that can be applied to any site under consideration. A remote-sensing solution, providing coverage over a wide area, is an attractive potential technology, which could be complemented by the coring-based solutions to provide ground truth data. As in many underwater remote-sensing problems, acoustics provides the most likely candidate modality. Successful implementation of an acoustic experiment that characterizes the shallow gassy seabed well would therefore be desirable. Whilst coring will remain intrinsically invasive, this paper outlines a short-range experiment, with sources and hydrophones on or in the seabed, that would indicate the feasibility of producing a remote system, even though this initial study involves invasive acoustic probes.

Acoustic characterization of gassy water has been well examined owing to its industrial, medical and oceanographic applications [28-33]. The corresponding experimental designs fall into two broad categories. The first category is based on the measurement of the compressional wave velocities and the attenuation coefficients from the transmission of pulses [34, 35]. In this category, the wave velocities are predominantly affected by the resonant bubble sizes and the attenuation in the medium is adequately attributed to the acoustic energy dissipated by bubbles through their scattering or extinction cross-section [35-38]. The second category is the dual-frequency insonification, which uses nonlinear mixing of frequencies employing a low pump frequency and a higher imaging frequency, concurrently [32, 39-45]. The received signals exhibit nonlinear scattered terms at the sum and difference frequencies as well as subharmonics [46-48] generated parametrically through Faraday waves on the bubble wall [49, 50]. For incoherent scattering, the amplitude of the scattered terms are proportional to the number of bubbles whose radius places them in a given discrete bin around a central value. An alternative approach (high frequency – high frequency insonification), where the difference between the frequencies corresponds to the resonant size of the bubbles being interrogated, has been successfully employed in Refs. [29, 41, 51], but is not used here. The rationale behind applying a varying pump frequency in both techniques is to capture the resonance effects at each discrete value of bubble radii, and thereafter to measure bubble populations [52]. Combination frequencies have only been used to study gassy marine sediments once before to the authors' knowledge (Tęgowski *et al*. [53, 54] taking spot-checks using specific echosounder frequencies rather than scanning across a frequency spectrum), and never *in situ* or in a rig that combines it with another acoustical method.

This combination-frequency technique is combined, in one apparatus, with the aforementioned propagation method (the measurement of sound speed and attenuation as pulses propagate along a buried array), following the principle that, since all methods of characterizing bubbles using acoustics have limitations, the use of two can be used to cross-check each other [48]. The use of two different experiment setups, which can be operated separately, though at the same location, will enable us to present acoustic propagation results from two different methods and compare them where applicable.

In this paper, we present the experimental details, processing techniques, *in situ* propagation results and supplementary laboratory measurements for sediment geotechnical properties at the experimental sites. The data are made available online, traceable using a DOI number (see Acknowledgements), so that any groups can attempt to fit them to appropriate forward models or invert them to estimate the bubble populations present. The use of two acoustic techniques (one linear, one nonlinear) measuring the same site is useful as it would enable two independent inversions, adding confidence if they agree [52].

II. THEORY

Many researchers [1-3, 44, 55-61] have studied acoustic wave propagation in gassy sediments. Highly complex variables of the problem such as nonlinear gas bubble dynamics, sediment rheology, porosity, grain size distribution, multiple scattering and the presence of multiple phases have led to slightly different formulations. In the current paper, the formulation in [3] (developed from [1] via [2] for this purpose) is most germane.

Let us assume plane wave propagation in a gassy sediment with non-uniform bubble size distribution. At a particular angular excitation frequency ω, the complex wavenumber k_m for the frequency domain wave propagation is given by [62]:

$$k_{\mathrm{m}}^2 = \frac{\omega^2}{c_{\mathrm{s}}^2} + 4\pi\omega^2 \int_0^\infty \frac{R_0 n(R_0)}{\omega_0^2 - \omega^2 + 2i\beta_{\mathrm{tot}}\omega} \mathrm{d}R_0 \,, \tag{1}$$

where, c_{s} is the compressional wave speed of the water-saturated (gas free) sediment, $n(R_0)\ \mathrm{d}R_0$ is the number of bubbles per unit volume with radii between R_0 and $R_0 + \mathrm{d}R_0$, ω_0 is the bubble resonance angular frequency, and β_{tot} is the total damping coefficient at each bubble radius. The phase velocity V and the attenuation A (dB/m) can be calculated as a function of the real and imaginary parts of the wavenumber, respectively, via:

$$V = \omega / Re\{k_{\mathrm{m}}\} \tag{2}$$

and

$$A = 8.6859\,|Im\,\{k_{\mathrm{m}}\}\,|. \tag{3}$$

The series of papers [1-3] develops a nonlinear model for the volume oscillations of gas bubbles in marine sediment, the small-amplitude expansion of which [3] produces the following explicit expression for the bubble resonance frequency:

$$\omega_0^2 = \left[3p_{\mathrm{g}_0} Re(\phi) - \frac{2\sigma\beta}{R_0} + 4G(1-\beta) + \frac{\omega^2 \rho R_0^2}{1 + (\omega R_0 / c_{\mathrm{s}})^2}\right] \Big/ m, \tag{4}$$

where p_{g_0} is the initial bubble interior pressure, ϕ is the gas thermodynamic parameter, σ is the surface tension at the gas-water interface, β is the porosity, G is the sediment shear modulus, and ρ is the density. The effective mass m in (4) is defined as:

$$m = \rho_{\mathrm{s}} R_0^2 + \frac{4\mu R_0}{c_{\mathrm{s}}} \tag{5}$$

with μ being the sediment viscosity. Ref. [3] explains the form and the derivation of the damping parameter β_{tot} and the gas thermodynamic parameter ϕ.

At a particular driving frequency, bubbles in steady-state that have their resonance frequency lower than the driving frequency undergo out-of-phase oscillations (the familiar inertia-controlled response, where the bubbles expand during the compressive half-cycle) and bubbles with resonance frequency higher than the driving frequency oscillate in-phase with the driving acoustic wave (the stiffness-controlled response) [28, 34]. The through-resonance transition between these two states occurs over a frequency band that narrows as the quality factor of the bubble in question increases. In this transition, greatly elevated or suppressed sound speeds may be observed when the excitation frequency is just above or below (respectively) the breathing-mode bubble resonance. The formulation of Ref. [3] displays these expected effects, and derives sound speed and attenuation formulae as given in (2) and (3), respectively, that converge, in the limit that there were no gas bubbles in the medium, to those of water-saturated sediment presented in Ref. [63].

Under the effect of an incident wave field, the total scattered pressure p_{sc} from an ensemble of oscillating gas bubbles within a small sensing volume V_{S} can be found from [64, 65]:

$$p_{\mathrm{sc}} \approx \int_{0}^{\infty} \frac{\rho R}{r}\left(\ddot{R}R + 2\dot{R}^{2}\right) n(R_0)\, \mathrm{d}R_0\,, \tag{6}$$

where is R the time-dependent pulsating radius of the bubble at each discrete initial bubble radius R_0 and r is the distance between the receiver and the center of the sensing volume.

III. EXPERIMENTAL SETUP

The two different forms of data, from transmission and combination frequency experiments, were collected using apparatus that shared many common components. This was designed to allow both data to be taken on the same day and same point of the tidal cycle without moving the rig. However, in this first deployment, the number of people on the team (e.g., to carry, dig and set up within the tidal window) was insufficient to accomplish such simultaneous measurements.

The rig was deployed at two sites offshore from Southampton, Hampshire U.K. within one to three hours after subaerial exposure. On each experiment date, the measurements were completed within a maximum of four to five hours' time intervals [24]. The experiment locations were selected to be within 20 m of a suitable dry point for the acquisition system. The exact experiment positions (pinned on a Google Map with GPS coordinates) and the execution times can be found in the electronic supplementary data file (see [66]), together with the ambient temperature and salinity values at the time of the experiments. Moreover, the water temperature data recorded in this region at 5-minute intervals in 2009 are provided in the electronic supplementary material [67]. Although such data are not available for 2008, the values in Ref. [67] show that the variations of water temperature, over a time frame of 4-5 hours during similar times of the year, are less than 0.4 °C. Kan *et al.* [68] present regression models (based on laboratory experiments) to predict the sound speed in sediments as a function of the ambient water temperature, and report that the ratio of sound speed in sediments to that in seawater remain almost unchanged as a function of temperature (see Fig. 5 therein).

A. Transmission rig

The experimental rig consisted of five acoustical components, i.e., one source transducer and four hydrophones, mounted on aluminum bars (Fig. 1). The transmission rig was designed so that the source (S) to receiver (R) separations could be adjusted for the sediment type under examination, e.g., in saturated muds much larger S-R separations can be used than in gassy muds with higher attenuation. The hydrophones were mounted at the end of 1-m-long rods made of carbon fiber with an acoustic impedance similar to that of the sediment. A slider rail lay on top of the sediment, and attached to it (with axes at 45° to the axis of the slider rail) were sliding supports for the carbon fiber rods. Once these supports were locked in position, they guided the carbon fiber rods with the 45° angle fixed, as they were inserted into the sediment. This ensured that the hydrophones lay on the acoustic axis of the source. The acoustic source was controlled by its own sliding support that was also attached to the axis of the slider rail with a 45° angle. A triangular hole was cut through which the source probe and the hydrophone array was inserted into the sediment at near 45°.

The acoustic pump source consisted of two elements, a low-frequency (LF) source (8-24 kHz) and a high-frequency (HF) source (26-120 kHz) (Neptune Sonar). The wet-end electronics were designed to impedance match the source to the amplifier by Blacknor Technology and were contained in a pressure cylinder approximately 0.6 m from the transducer. Although initial calibration documents were received, additional calibrations of source levels were performed in order to include the effects of the wet-end matching. The measured source levels varied from 200 to 213 dB re 1 $\mu\text{Pa} \cdot \text{m}$ (zero-to-peak) for 26-120 kHz frequency range. A BLK 1264 pump amplifier with a 3.5 V peak-to-peak voltage input was used in calibration tests.

The four receivers attached to the carbon fiber poles were D140 hydrophones (from Neptune Sonar) modified with encasing material that provided additional protection for insertion into sediment. The sensitivity of the receivers varied from -209 to -217 dB re 1 $\text{V} \cdot \mu\text{Pa}^{-1}$ from 2 to 100 kHz. The hydrophones had a wet-end amplifier (supplied by the manufacturer) located approximately 0.5 m from the receiver. Amplification was applied at both the wet and dry ends in three stages with adjustable gains.

The next stage involved setting up the connections with the acquisition system and sending out a series of test signals using the acquisition code written in MATLAB software. The frequency was increased in 2-kHz steps from 8 to 100 kHz. The duration of the pulses transmitted from the pump source was set as 1 ms for the majority of the sets, and was set as 20 acoustic cycles for the remainder of the sets (as stated in Supplemental material). Specific values of the source amplitudes and waveforms for each set can be found in Sec. IV of Ref. [66]. The signal generation and data acquisition were conducted at a sampling frequency of 2 MHz. At each frequency, a number of pulses were emitted (i.e. 10 to 40) with 4-ms pauses between pulses to avoid reverberation. This procedure ensured a reliable data set in which the standard deviation of the measured sound speed and attenuation values could be reduced by applying stacking-based post-processing. The data were analyzed from pairs of adjacent hydrophones, i.e., the pairs 1-2, 2-3 and 3-4.

B. Combination frequency apparatus

The combination frequency experiment used the same sliding rod rig as described in the previous section (Fig. 1). However, whereas the experiment in the previous section made use only one of the two projectors (the pump source), in this experiment the second projector (the imaging source) was simultaneously used. Moreover, instead of the hydrophone array (R1-R4), the imaging receiver was used to collect the received signals.

In this way, the two-frequency technique employed simultaneous insonification of the bubble population with a lower frequency signal f_p (pump frequency) and a higher frequency signal f_i (the imaging frequency). The imaging source and receiver had a common focal point, where their acoustic axes intersected each other at 90°, the axes being 45° either side of the acoustic center line of the pump transmitter. Figs. 1 and 2 in Ref. [69] present side and plan views of the combination frequency experiment rig.

Setting up a correct measurement environment with accurate parameters was somewhat more complicated when adding in the combination frequency experiment than in the transmission experiment alone. In the transmission case, all the receivers lay along the acoustic axis of the source and the losses were computed from the amplitudes of the signals measured on the hydrophones. For the case of combination frequency experiment, however, it was necessary to calculate the sensing (insonification) volume, which lay at the beam overlap of the pump and the imaging-frequency transducers. The beam patterns of the transmitters were computed simultaneously and were overlapped to determine a region in which the resultant sound pressure level falls off only a pre-set amount (e.g. 3 dB) of its maximum value. Because the pump frequency was varied, the beam pattern for that transducer varied, thus changing the sensing volume. This change made it necessary to repeat the sensing volume calculation for each pump frequency

The beam patterns of both the imaging source and receivers were provided by the manufacturer, but they were valid for in-water operating conditions. Therefore, in order to simulate the pressure fields in sediments, a numerical algorithm was developed using the impulse response method [70]. The method was first verified against water tank measurements and the simulations of *in situ* pressure fields were performed inputting the appropriate density, sound speed and drive frequency values. The differences in the computed pressure values lay within 0 – 2.5 dB over a length of ~6 m for compressional wave speeds from 1470 to 1800 $\text{m}\cdot\text{s}^{-1}$ in sediment samples (for further details see [71, 72]).

The combination frequency experiments were conducted keeping the imaging frequency f_i constant at 220 kHz and varying the pump frequency f_p from 8 kHz to 24 kHz, from 20 kHz to 40 kHz, and from 30 kHz to 100 kHz, all in 2-kHz increments. The acoustic sources were adjusted such that at the focus point of the rig, the pressure stayed constant at 15 kPa (zero-to-peak amplitude) for all frequencies. This value was set as the calibration pressure. The two signals were generated as 1 ms square pulses (see Sec. V of Ref. [64] for further details). The scattered signal was recorded using a sampling frequency of 2 MHz. Simulations showed that the pulse length was long enough for the bubbles to reach steady state.

IV. SIGNAL PROCESSING

The four receivers used in the transmission experiment were identical within our measurement capabilities, and the data were processed by selecting specific pairs of receivers.

For instance, the coupling between the sediment and the receiver could be taken as identical assuming that the physical properties of the sediment such as porosity, mean grain size and silt/clay content do not change greatly over the length scales encountered in the experiment (~15–20 cm receiver separations for the rig considered). Moreover, the time delays incurred by the electronic components of the devices and due to the casing of the hydrophones could be regarded as equal because the channels used the same materials and shared common acquisition electronics.

The characteristics of the emitted acoustic waves were first tested in water tank calibration trials in order to investigate the variability and the noise events. The FFT results showed that the central frequency of the output signal from the transducer lies within 1% of the input signal to the function generator device. Furthermore, the signals recorded by the receivers exhibited central frequencies within 3% of the transducer output signals.

The signals were processed through two stages of filtering. The first stage removed dominant noise sources for the different frequency ranges (a low pass filter at 35 kHz was used for frequencies between 26 and 30 kHz whilst for the other frequencies a wide band 10-300 kHz band-pass filter was applied). In the second stage, a digital Butterworth filter of fifth order was applied with the center frequency selected to match the outgoing signal and the bandwidth chosen to match the 6 dB levels of the signal's spectrum as measured in the water tanks tests.

The received signals were post-processed with stacking in order to increase the signal-to-noise ratios (SNR). Identical processing was applied to all channels in order not to bias the computed velocity and attenuation values. The use of a median stack results in a SNR enhancement S_n given as [73]

$$S_n = \sqrt{\frac{2N_s}{\pi}} \ , \tag{7}$$

where N_s is the number of shots applied. Here N_s is 20 or 30, resulting in a SNR enhancement, as measured on a linear scale, of 3.57 or 4.37, respectively. An example of a filtered and median-stacked signal pair is shown in Fig. E2 in Sec. VI of the electronic supplementary file [66].

Subsequent to stacking the waveforms, the envelope of the signal $y(t)$ was computed using

$$\zeta(t) = |\hat{y}(t)|, \tag{8}$$

where $\hat{y}(t)$ is the analytic form of $y(t)$, whose imaginary component is the Hilbert transform of $y(t)$:

$$\hat{y}(t) = y(t) + i\,y(t) * \frac{1}{\pi t}, \tag{9}$$

with * representing the convolution operation. The signal pair as in Fig. E2b and E2c in [66] can be then used to determine the group and phase velocity and the attenuation of the acoustic waves in gassy sediment.

The group velocity in the sediment was estimated by computing the time delay between the pulses received on two hydrophones separated by a known distance. The time delay was computed using the cross-correlation function [74]. A method based on the envelopes of the signals was preferred. First, a reference envelope was formed by computing Eq. (8) for the first signal and applying an amplitude threshold. Then the correlations of the envelopes of the two hydrophone signals with the reference envelope were computed (see Fig. E3 in [66]).

The attenuation of the acoustic waves was evaluated by comparing the amplitudes of the signal envelopes. The amplitude of the received pulse was estimated using the central portion of the pulse, which is unaffected by ring-up or ring-down. For instance, for a signal with 1-ms duration, the amplitude of the middle 0.5-ms section was computed and for signals with 20 oscillations, the average amplitude of the middle 10 oscillations was calculated. The attenuation was found by comparing the average of these amplitudes across multiple pulses. Further corrections owing to the spreading losses, the amplification gains and the receiver sensitivities were applied to determine the final values of attenuation.

For the combination frequency insonification, the signal processing was straightforward. At each pump frequency, the Fourier transform of the received signal was calculated and then corrected by the receiver sensitivity, to give the pressure amplitude at the pump, difference and sum frequencies.

V. LABORATORY AND FIELD MEASUREMENTS

The theoretical model in Sec. II requires input values for the water-saturated sediment such as the density, shear modulus, viscosity, and the compressional wave speed. In order to obtain accurate values of these parameters, laboratory measurements on the pressurized core samples collected from the sites were carried out; the viscosity of the sediment was taken from the previous studies that investigated the rheological behavior of gassy mud [75, 76]. The permeability and tortuosity values of sediment were taken as in Ref. [24]. The experiments took place one to three hours after subaerial exposure. The measured density (ρ=1640 $\pm$ 50 kg$\cdot$ m^{-3}) suggested a value for sediment porosity between 60% and 70%.

The experiment locations were two intertidal sites on the south coast of England: Calshot in Southampton Water and the Mercury marina in the Hamble estuary. The seafloor sediments at these locations fall into the broad category of muddy sediments, but the grain size distribution and the organic content of these two locations were different. The sediment characteristics for these locations are given in Table 1.

The *p*-wave velocity measurements on the split core were conducted in the laboratory at 500 kHz. The rationale behind employing an ultrasonic frequency much greater than the likely resonances of the bubbles in the medium is that the bubble pulsations at this range become inertia-controlled and in-phase with the acoustic field, and thus have diminished effects on the phase velocity in the medium [64]. Therefore, the compressional wave velocity obtained in this way can be used conveniently as the value of the saturated (gas-free) sediment. The core length from the Calshot location was 50 cm and the measurements were obtained at 2-cm intervals starting at a core depth of 7 cm. The measured ultrasonic *p*-wave velocity varied between 1430 $\mathrm{m \cdot s^{-1}}$ and 1550 $\mathrm{m \cdot s^{-1}}$, showing less variability compared to the *in situ* measurements that were performed at lower frequencies and included bubble resonance effects (Section VI).

Subsequent to the ultrasonic *p*-wave measurements, shear wave velocity measurements were conducted on the split core in order to estimate the sediment shear modulus. This was accomplished by inserting bender elements with 10 cm separation in the core. Only the muddy homogeneous part of the core was of interest, because backscatter data from sandy layers could not be received. The average measured velocity was 40 $\mathrm{m \cdot s^{-1}}$ at 2 kHz, which yielded an average estimation of 2.62 MPa for the shear modulus (*G*).

Although the value for *G* was found by direct measurements on split cores with residual fabrics left behind by *in situ* gas, we assumed that the gas-free sediment shear modulus has the same value. Hence, we relied on the fact that the presence of gas has little impact on shear wave velocity, especially when compared to the impact of gas on compressional wave propagation [77]. Laboratory measurements in kaolin containing methane bubbles confirmed the low impact of the gas presence on the sediment shear modulus when small strains, such as those induced by acoustic excitation, are involved [78].

Core transmission wave measurements for the Mercury site were carried out at 500 kHz in the same manner as for the Calshot site. The core length was 40 cm and measurements were made from the top 8 cm to the bottom of the core at 2-cm intervals. The results indicated a compressional wave velocity value of $1415 \pm 20\ \mathrm{m \cdot s^{-1}}$.

Visual inspection of the split cores (see Fig. 2a and 2b) also provided substantial information for the characteristics of the samples. The upper part (first 25–30 cm) of the Calshot core consisted of thin sandy layers overlying grey mud, where more gas pockets were observed as the depth increased. The sandy sediments observed between 25 - 30 cm in the upper section of the core was consistent with the higher in situ p-wave speeds measured between hydrophones 1-2 at 21 - 35 cm depth. Observation of the Mercury core profile (Fig. 2b) revealed a significant number of gas pockets, increasing with depth, with relatively larger sizes. Furthermore, the sediment composition exhibited more homogeneity with no distinct horizontal layers as the depth increased.

VI. TRANSMISSION PROPAGATION RESULTS

In this section, we present the acoustic propagation results, i.e., the sediment compressional wave speed and attenuation, obtained from the transmission experiments using the rig shown in Fig. 1. As explained in Sec. III, measurements were conducted by sending pulses at frequencies from 8 kHz to 24 kHz, and from 26 kHz to 100 kHz, in 2-kHz steps. For nominal values of *ca.* 2.6 MPa for the shear modulus and 60 % for the porosity of the sediment, Eq. (4) indicates that the gas resonance effects for the bubble size range $R_0 = [130, 980]$ μm could be determined.

A. The Calshot site

The measurements at the Calshot site took place during different seasons, on three separate occasions: 10 April 2008 (four sets), 10 June 2008 (one set) and 04 August 2008 (twelve sets). On each day, several sets of measurements were carried out, and a number of shots (20 or 30) were acquired in each set. The complete data regarding the sound speed and attenuation were written to Excel files (see the supplementary material [79]).

As an illustrative example, the *in situ* transmission results from 10 April 2008 are shown in Fig. 3. The unbroken black line represents results from the first hydrophone pair (hydrophone 1 and 2) and the red dashed line from the second hydrophone pair (hydrophones 2 and 3). The *in situ* results from the first hydrophone pair gave a mean value for the sound speed of 1724 $\mathrm{m \cdot s^{-1}}$ with standard deviation of 99 $\mathrm{m \cdot s^{-1}}$. If a linear relationship between the attenuation and frequency were assumed based on Hamilton's formulation [80], the best-fit line would have resulted in k = 0.83 $\mathrm{dB \cdot m^{-1} \cdot kHz^{-1}}$ with a R_{d}^2 (coefficient of determination [73]) value of 0.98 (Figs. 3 and 4 both plot the 'equivalent plane wave attenuation of the gassy sediment', i.e., after spreading losses have been subtracted, but we have not subtracted the attenuation of bubble-free sediment).

The second hydrophone pair measured an average sound speed of 1346 $\mathrm{m \cdot s^{-1}}$ with standard deviation of 71 $\mathrm{m \cdot s^{-1}}$. Assuming a linear dependence of attenuation with frequency, a line with a slope of k = 0.72 $\mathrm{dB \cdot m^{-1} \cdot kHz^{-1}}$ and R_{d}^2 =0.98 could be fitted to the results (the statistical uncertainty values calculated for the group velocity and attenuation in all transmission experiments can be found in the electronic supplementary file [79]). The difference in sound speed measured by the two hydrophone pairs indicated differences in the sediment composition. Based on literature values for *p*-wave values in muddy and sandy sediments, it could be concluded that the sand content was higher in the area of the first pair of hydrophones.

The value of k for the muddy sediment below the sandy layer (~0.7 $\mathrm{dB \cdot m^{-1} \cdot kHz^{-1}}$) was approximately one order of magnitude higher than that encountered in the literature for gas-free muddy sediments [80, 81]. This was strong evidence of gas presence, because the attenuation across all frequencies increases significantly even in the presence of minute amounts of gas [2, 56, 82]. Furthermore, the sound speed observed in the mud was lower than values typical of muddy gas-free sediments.

B. The Mercury site

In-situ transmission measurements at the Mercury intertidal site were carried out using the same materials and methods as for the Calshot site. The measurements took place at different times of the year. On 15 April 2008, the apparatus was deployed twice, at two positions that were approximately two meters away from one another (that were named as 'lower pitch' and 'upper pitch' in the data), in order to enhance the spatial variety of the results. Eight sets of data were collected at the lower pitch and another eight sets were collected at the upper pitch. Six sets of transmission data were collected on 11 June 2008. Velocity and attenuation results were written to Excel files (see [79]). As an example, the propagation results from the first set from 11 June 2008 are shown in Fig. 4. The solid black lines represent the group velocity and attenuation from the first hydrophone pair (hydrophone 1 and 2) and the red dashed lines from the second hydrophone pair (hydrophones 2 and 3). The first hydrophone pair measured an average sound speed of 1323 $\mathrm{m \cdot s^{-1}}$ with a standard deviation of 110 $\mathrm{m \cdot s^{-1}}$. If a linear dependence of attenuation with frequency were to be fitted to these data, the value of *k* would have been equal to 0.78 $\mathrm{dB \cdot m^{-1} \cdot kHz^{-1}}$ (with $R_\mathrm{d}^2 = 0.89$). An average sound speed of 1250 $\mathrm{m \cdot s^{-1}}$ with a standard deviation of 240 $\mathrm{m \cdot s^{-1}}$ was obtained from the hydrophone pair 2-3. Assuming again a linear dependence of attenuation with frequency, the value of *k* was equal to 1.30 $\mathrm{dB \cdot m^{-1} \cdot kHz^{-1}}$ (with $R_\mathrm{d}^2 = 0.92$). Moreover, a dispersion in the sound speed was observed at particular excitation frequencies, i.e. at 26 kHz, 70 kHz and 98 kHz. These alterations to the sound speed and the high values of attenuation were attributed to the breathing mode resonance effects caused by gas bubbles, described in Sec. II, and were strong evidence for the presence of gas.

VII. COMBINATION FREQUENCY RESULTS

The combination frequency experiments took place at the Hamble site on two different dates – 25 August 2008 (15 sets) and 28 August 2008 (21 sets), and at the Calshot site on 23 July 2008 (8 sets). The measurements were conducted using a low-frequency pump source (8-24 kHz range), a medium-frequency pump source (20-40 kHz) and a high-frequency pump source (30-100 kHz), all in 2-kHz increments. The imaging frequency was set as f_i = 220 kHz for all measurements. Specific values of the source amplitudes for each measurement set were given in Sec. V of the supplementary file [66].

The assessment of the results of the combination frequency experiments is slightly different from that of the transmission experiments. The scattered acoustic pressure waves from an ensemble of bubbles in a sensing volume at a given distance, that propagate as a result of the pulsations of the bubbles (see Eq. (6)), need to be considered. Note that Eq. (6) considers implicitly the attenuation through the path from the sensing volume to the receiver in the gassy sediment. At a particular pump frequency f_p, nonlinear harmonics are generated because of the multiple-frequency insonification, i.e. at the difference frequency $(f_i - f_p)$, the sum frequency $(f_i + f_p)$ and the second harmonic of the pump frequency $(2\ f_p)$. The latter property indicates that the gassy sediment was interrogated with a broader frequency range in comparison to the transmission experiment. The amplitudes of the spectral components at these frequencies are different from each other. However, they are proportional to the pressure amplitudes of the pump source and the image source (explicit analytical expressions for these are not given here, but can be found in [39, 40]). Note that the pressure amplitudes for the pump and imaging frequency transducers were calibrated in water tank tests. In gassy sediment, the amplitudes of the waves attenuate from the acoustic source to the sensing volume based on the transmission principle. The nonlinear propagation model (eq. 6) and the source amplitudes designed in the experiment can be used to infer the bubble population in sediment, which can be then used to account for the reduction in amplitude of the pump and imaging beams in the sensing volume (where they could not be measured invasively because it would disturb the bubble population there). Therefore, the full range of insonification frequencies, their harmonics, and the spectral amplitudes at these frequencies can be considered simultaneously, if an appropriate forward model were to be fitted to the experimental results.

Fig. 5 shows the acoustic time history recorded by the receiver during an insonification with pump frequency f_p = 44 kHz, and its corresponding spectrogram. The data are embedded into the figure from the measurement set 6 from 23 July 2008 in Calshot. One may observe the distinct spectral components at certain frequencies such as $f_p,\ 2f_p,\ f_i + f_p$= 266 kHz, etc. Fig. 6 shows all the pressure amplitude results from set 6 from 23 July 2008 as a function of the full range of pump frequencies, and the corresponding difference frequency and sum frequency ranges. The average values of the pressure amplitudes are found from the repeated insonifications. The data regarding the scattered pressure amplitudes obtained in all three experiment locations are provided as supplementary material [83].

VIII. CONCLUSIONS

Acoustic propagation experiments were carried out in intertidal marine sediments in Southampton Water and Hamble River areas to gain insights into the acoustic characterization of gassy mud. For this purpose, a sophisticated experimental rig was designed and deployed *in situ*. The first component of the setup was a transmission arrangement consisting of a source transducer and four hydrophone receivers; whereas, the second component consisted of a receiver and two sources (one from the previous experiment) that operated simultaneously to expose nonlinearly generated harmonics of the gas bubbles. The resonant bubble size corresponding to the frequency range used, was 130-980 μm, assuming a nominal value of *ca.* 2.6 MPa for the shear modulus of the sediments. The attenuation values obtained from the transmission experiments ranged from 6 $\mathrm{dB \cdot m^{-1}}$ to 27 $\mathrm{dB \cdot m^{-1}}$ at the lowest frequency (8 kHz) and from 15 $\mathrm{dB \cdot m^{-1}}$ to 175 $\mathrm{dB \cdot m^{-1}}$ at the highest frequency (100 kHz), exhibiting a maximum value of 210 $\mathrm{dB \cdot m^{-1}}$ at intermediate drive frequencies. Furthermore, the pressure amplitudes at the location of the receiver for the combination rig were of the order of ~10-20 kPa at the pump frequency and ~50-100 Pa at the difference and sum frequencies.

Additional laboratory analyses were performed on sediment core samples that gave supporting information on the geotechnical properties of the sites under investigation. This included the measurement of ultrasonic compressional wave velocity as a function of depth, shear wave velocity and the visual observations of split cores. The compressional wave speed values exhibit a depth gradient along with the attenuation values as measured with the transmission experiment rig. The gas pockets observed from the split cores also indicated a gassier occurrence at the Mercury site, which is in accordance with the results obtained from the transmission pulses.

The linear-fit curves of the attenuation results from the two different muddy sites indicated attenuation that was at least one order of magnitude higher than that of water-saturated sediments, which is a strong indication of the presence of gas.

We used the intertidal zone to undertake the first test deployments of novel sensors because of its ready accessibility. However, gas populations in the intertidal zone sediments are important for study in their own right; for example, there are likely acoustical implications for the sound transmitted to benthic species from anthropogenic activity.

In the early days of marine sediment acoustics, studies of gas-free sediments were more common than those of gassy sediments, where the presence of gas complicated modelling and measurements [84-87]. Now, as studies of gas populations in gassy-sediments that are not subject to tidal exposures become established [4-13], it is timely to look at forward modeling for gassy intertidal sediments, and collect data suitable for acoustic inversion studies. The intertidal zone, with its specialized flora and fauna, and frequent proximity to anthropogenic factors (dredging, shipping and invasive species, civil engineering, chemical and acoustic pollutants etc.) can make it a vulnerable habitat, yet it is one whose biodiversity is critical to keeping it healthy [84, 88]. The presence of high gas void fractions, and great variability in space and time, make intertidal zones complex regions to study (especially ones that are exposed to atmosphere during the tidal cycle, as occurred here). There are large diurnal changes of temperature, salinity and gas content, the variation from maximum to minimum hydrostatic head being a large fraction of the maximum absolute pressure on the sediment, a pressure that affects gas dissolution, exsolution, and bubbling from the sediment. Particularly, the effect of temperature, and its gradient with depth, on the sound propagation can be accounted for using the models and results presented in [89, 90]. As acoustic techniques develop to provide finer spatial and temporal resolution of the acoustic environment and bubble population, and correlate these to monitoring the benthic species and their interaction with the environment, the health of intertidal zones can be better monitored and protected.

Overall, our results provide acoustical datasets suitable for detailed inversion studies of gas bubble populations using linear and non-linear acoustic bubble theory. The presence of gas in these intertidal muddy sediments has been established from core analyses and *in situ* acoustic velocity and attenuation measurements.

Acknowledgements

This work is funded by the Engineering and Physical Sciences Research Council (grant EP/D000580/1, Principal Investigator T.G. Leighton), with support for further analysis of data from the National Environment Research Council UK (Grant number NE/J022403/1, Principal Investigator T.G. Leighton). Data (doi: 10.5258/SOTON/D1937) can be found at https://doi.org/10.5258/SOTON/D1937.

REFERENCES

[1] T. G. Leighton, "Theory for acoustic propagation in marine sediment containing gas bubbles which may pulsate in a non-stationary nonlinear model," *Geophysical Research Letters,* vol. 34, p. L17607, 2007.

[2] A. Mantouka, H. Dogan, P. R. White and T. G. Leighton, "Modelling acoustic scattering, sound speed, and attenuation in gassy soft marine sediments," *J. Acoust. Soc. Am.,* vol. 140, no. 1, pp. 274-282, 2016.

[3] H. Dogan, P. R. White and T. G. Leighton, "Acoustic propagation in gassy porous marine sediments: The rheological and the elastic effects," *J. Acoust. Soc. Am.,* vol. 141, no. 3, pp. 2277-2288, 2017.

[4] J. Locat and J. Mienert, Submarine mass movements and their consequences, Dordrecht, The Netherlands: Kluwer, 2003, pp. 1-542.

[5] A. G. Judd and M. Hovland, "The evidence of shallow gas in marine sediments," *Continental Shelf Research,* vol. 12, pp. 1081-1095, 1992.

[6] P. Fleischer, T. H. Orsi and M. D. Richardson, "Distribution of free gas in marine sediments: a global overview," *Geo-Marine Letters,* vol. 21, pp. 103-122, 2001.

[7] G. R. Venegas, A. F. Rahman, K. M. Lee, M. S. Ballard and P. S. Wilson, "Toward the Ultrasonic Sensing of Organic Carbon in Seagrass-Bearing Sediments," *Geophysical Research Letters,* vol. 46, no. 11, pp. 5968-5977, 2019.

[8] P. Feldens, I. Schulze, S. Papenmeier, M. Schönke and J. S. von Diemling, "Improved Interpretation of Marine Sedimentary Environments Using Multi-Frequency Multibeam Backscatter Data," *Geosciences,* vol. 8, no. 214, pp. 1-14, 2018.

[9] G. C. Sills and S. J. Wheeler, "The significance of gas for offshore operations," *Continental Shelf Research,* vol. 12, no. 10, pp. 1239-1250, 1992.

[10] J. Blackford, H. Stahl, J. M. Bull, B. J. P. Bergès, M. Cevatoglu, A. Lichtschlag, D. Connelly, R. H. James, J. Kita, D. Long, M. Naylor, K. Shitashima, D. Smith, P. Taylor, I. Wright, M. Akhurst, B. Chen, T. M. Gernon, C. Hauton, M. Hayashi, H. Kaieda, T. G. Leighton, T. Sato, M. D. J. Sayer, M. Suzumura, K. Tait, M. E. Vardy, P. R. White and S. Widdicombe, "Detection and impacts of leakage from sub-seafloor deep geological carbon dioxide storage," *Nature Climate Change,* vol. 4, pp. 1011-1016, 2014.

[11] B. J. P. Berges, T. G. Leighton and P. R. White, "Passive acoustic quantification of gas fluxes during controlled gas release experiments," *International Journal of Greenhouse Gas Control,* vol. 38, pp. 64-79, 2015.

[12] J. Li, P. White, J. M. Bull and T. M. Leighton, "A noise impact assessment model for passive acoustic measurements of seabed gas fluxes," *Ocean Engineering,* vol. 183, pp. 294-304, 2019.

[13] J. Blackford, J. M. Bull, M. Cevatoglu, D. Connelly, C. Hauton, R. H. James, A. Lichtschlag, H. Stahl, S. Widdicombe and I. C. Wright, "Marine baseline and monitoring strategies for Carbon Dioxide Capture and Storage (CCS)," *International Journal of Greenhouse Gas Control,* vol. 38, pp. 221-229, 2015.

[14] A. G. Judd, M. Hovland, L. I. Dimitrov, S. G. Gil and V. Jukes, "The geological methane budget at Continental Margins and its influence on climate change," *Geofluids,* vol. 2, pp. 109-126, 2002.

[15] T. G. Leighton and P. R. White, "Quantification of undersea gas leaks from carbon capture and storage facilities, from pipelines and from methane seeps, by their acoustic emissions," *Proceedings of the Royal Society A - Mathematical, Physical and Engineering Sciences,* vol. 468, pp. 485-510, 2012.

[16] S. Ker, L. Y. Gonidec, B. Marsset, G. K. Westbrook, D. Gibert and T. A. Minshull, "Fine-scale gas distribution in marine sediments assessed from deep-towed seismic data," *Geophysical Journal International,* vol. 196, pp. 1466-1470, 2014.

[17] J. R. Schubel, "Gas bubbles and the acoustically impenetrable or turbid character of some estuarine sediments," in *Natural Gases in Marine Sediments*, I. R. Kaplan, Ed., New York, Plenum, 1974, pp. 275-298.

[18] T. G. Leighton and G. Robb, "Preliminary mapping of void fractions and sound speeds in gassy marine sediments from subbottom profiles," *Journal of the Acoustical Society of America,* vol. 124, no. 5, pp. EL313-EL320, 2008.

[19] E. Uzhansky, B. Katsnelson, A. Lunkov and I. Ostrovsky, "Spatial and temporal variability of free gas content in shallow sediments: Lake Kinneret as a case study," *Geo-Marine Letters,* vol. 40, pp. 491-505, 2020.

[20] O. Thießen, M. Schmidt, F. Theilen, M. Schmitt and G. Klein, "Methane formation and distribution of acoustic turbidity in organic-rich surface sediments in the Arkona Basin, Baltic Sea," *Continental Shelf Research,* vol. 26, pp. 2469-2483, 2006.

[21] F. Abegg and A. L. Anderson, "The acoustic turbid layer in muddy sediments of Eckernforde Bay, Western Baltic: methane concentration, saturation and bubble characteristics," *Marine Geology,* vol. 137, pp. 137-147, 1997.

[22] A. L. Anderson, F. Abegg, J. A. Hawkins, M. E. Duncan and A. P. Lyons, "Bubble populations and acoustic interaction with the gassy floor of Eckernforde Bay," *Continental Shelf Research,* vol. 18, pp. 1807-1838., 1998.

[23] A. P. Lyons, M. E. Duncan and A. L. Anderson, "Predictions of the acoustic scattering response of free-methane bubbles in muddy sediments," *J. Acoust. Soc. Am.,* vol. 99, no. 1, pp. 163-172, 1996.

[24] A. I. Best, M. D. J. Tuffin, D. J. K. and J. M. Bull, "Tidal height and frequency dependence of acoustic velocity and attenuation in shallow gassy marine sediments," *Journal of Geophysical Research,* vol. 109, no. B8, p. B08101, 2004.

[25] A. H. Reed, B. P. Boudreau, C. Algar and Y. Furukawa, "Morphology of gas bubbles in mud: A microcomputed tomographic evaluation," in *Underwater Acoustic Measurements: Technonlogies and Results*, 2005.

[26] A. Brodecka, P. Majewski, J. Bolalek and Z. Klusek, "Geochemical and acoustic evidence for the occurence of methane in sediments of the Polish sector of the southern Baltic sea," *Oceanologia,* vol. 55, no. 4, pp. 951-978, 2013.

[27] S. Garcia-Gil, E. de Blas, N. Martinez-Carreno, J. Iglesias, R. Rial-Otero, J. Simal-Gandara and A. G. Judd, "Characterisation and preliminary quantification of methane reservoir in a coastal sedimentary source: San Simon Bay, Ria de Vigo, NW Spain," *Estuarine, Coastal and Shelf Science,* vol. 91, pp. 232-242, 2011.

[28] T. G. Leighton, "What is ultrasound?," *Progress in Biophysics and Molecular Biology,* vol. 9, no. 1-3, pp. 3-83, 2007.

[29] T. G. Leighton, "From seas to surgeries, from babbling brooks to baby scans: The acoustics of gas bubbles in liquids," *International Journal of Modern Physics B,* vol. 18, no. 25, pp. 3267-3314, 2004.

[30] I. M. Brooks, M. J. Yelland, R. C. Upstill-Goddard, P. D. Nightingale, S. Archer, E. D'Asaro, R. Beale, C. Beatty, B. Blomquist, A. A. Bloom, B. J. Brooks, J. Cluderay, D. Coles, J. Dacey, M. DeGrandpre, J. Dixon, W. M. Drennan, J. Gabriele, L. Goldson, N. Hardman-Mountford, M. K. Hill, M. Horn, P. –C. Hsueh, B. Huebert, G. de Leeuwuw, T. G. Leighton, M. Liddicicoat, J. J. N. Lingard, C. McNeil, J. B. McQuaid, B. I. Moat, G. Moore, C. Neill, S. J. Norris, S. O`Doherty, R. W. Pascal, J. Prytherch, M. Rebozo, E. Sahlee, M. Salter, U. Schuster, I. Skjelvan, H. Slagter, M. H. Smith, P. D. Smith, M. Srokosz, J. A. Stephens, P. K. Taylor, M. Telszewski, R. Walsh, B. Ward, D. K. Woolf, D. Young and H. Zemmelink, "Physical exchanges at the air sea interface: UK SOLAS field measurements," *Bulletin of the American Meteorological Society,* vol. 90, pp. 629-644, 2009.

[31] T. G. Leighton, D. G. H. Coles, M. Srokosz, P. R. White and D. K. Woolf, "Asymmetric transfer of CO2 across a broken sea surface," *Scientific Reports,* vol. 8:8301, pp. 1-9, 2018.

[32] A. D. Phelps and T. G. Leighton, "Oceanic bubble population measurements using a buoy-deployed combination frequency technique," *IEEE J. Oceanic Eng.,* vol. 23, pp. 400-410, 1998.

[33] A. J. Sojahrood, Q. Li, R. Karshafian, T. M. Porter and M. Kolios, "Investigation of the nonlinear propagation of ultrasound through a bubbly medium including multiple scattering and bubble-bubble interaction: Theory and experiment," in *IEEE International Ultrasonics Symposium (IUS)*, Washington, 2017.

[34] T. G. Leighton, S. D. Meers and P. R. White, "Propagation through nonlinear time-dependent bubble clouds and the estimation of bubble populations from measured acoustic characteristics," *Proc. R. Soc. Lond. A,* vol. 460, no. 2049, pp. 2521-2550, 2004.

[35] K. W. Commander and R. J. McDonald, "Finite-element solution of the inverse problem in bubble swarm acoustics," *J. Acoust. Soc. Am.,* vol. 89, pp. 592-597, 1991.

[36] M. A. Ainslie and T. G. Leighton, "Near resonant bubble acoustic cross-section corrections, including examples from oceanography, volcanology, and biomedical ultrasound," *J. Acoust. Soc. Am.,* vol. 126, no. 5, pp. 2163-2175, 2009.

[37] M. A. Ainslie and T. G. Leighton, "Review of scattering and extinction cross-sections, damping factors, and resonance frequencies of a spherical gas bubble," *Journal of Acoustical Society of America,* vol. 130, no. 5, pp. 3184-3208, 2011.

[38] R. Duraiswami, S. Prabhukumar and G. L. Chahine, "Bubble counting using an inverse acoustic scattering method," *J. Acoust. Soc. Am,* vol. 104, pp. 2699-2717, 1998.

[39] E. A. Zabolotskaya and S. I. Soluyan, "Emission of harmonic and combination-frequency waves by air bubbles," *Sov. Phys. Acoust*, vol. 18, pp. 396-398, 1973.

[40] V. L. Newhouse and P. M. Shankar, "Bubble size measurements using the nonlinear mixing of two frequencies," *J. Acoust. Soc. Am.,* vol. 75, no. 5, pp. 1473-1477, 1984.

[41] A. M. Sutin, S. W. Yoon, E. J. Kim and I. N. Didenkulov, "Nonlinear acoustic method for bubble density measurements in water," *J. Acoust. Soc. Am.,* vol. 103, no. 5, pp. 2377-2384, 1998.

[42] T. G. Leighton, R. J. Lingard, A. J. Walton and J. E. Field, "Acoustic bubble sizing by the combination of subharmonic emissions with an imaging frequency," *Ultrasonics,* vol. 29, pp. 319-323, 1991.

[43] A. D. Phelps, D. G. Ramble and T. G. Leighton, "The use of a combination frequency technique to measure the surf zone bubble population," *Journal of the Acoustical Society of America,* vol. 101, no. 4, pp. 1981-1989, 1997.

[44] F. A. Boyle and N. P. Chotiros, "Nonlinear acoustic scattering from a gassy poroelastic seabed," vol. 103, pp. 1328-1336, 1998.

[45] M. Cavaro, C. Payan and J. Moysan, "Microbubble cloud characterization by nonlinear frequency mixing," *Journal of the Acoustical Society of America,* vol. 129, pp. EL179-183, 2011.

[46] T. G. Leighton, D. G. Ramble, A. D. Phelps, C. L. Morfey and P. P. Harris, "Acoustic detection of gas bubbles in a pipe," *Acustica,* vol. 84, no. 5, pp. 801-814, 1998.

[47] A. D. Phelps and T. G. Leighton, "High-resolution bubble sizing through detection of the subharmonic response with a two frequency excitation technique," *Journal of the Acoustical Society of America,* vol. 99, pp. 1985-1992, 1996.

[48] T. G. Leighton, A. D. Phelps, D. G. Ramble and D. A. Sharpe, "Comparison of the abilities of eight acoustic techniques to detect and size a single bubble," *Ultrasonics,* vol. 34, pp. 661-667, 1996.

[49] A. O. Maksimov and T. G. Leighton, "Transient processes near the threshold of acoustically driven bubble shape oscillations," *Acta Acustica,* vol. 87, no. 3, pp. 322-332, 2001.

[50] A. D. Phelps and T. G. Leighton, "The subharmonic oscillations and combination-frequency emissions from a resonant bubble: their properties and generation mechanisms," *Acta Acustica,* vol. 83, pp. 59-66, 1997.

[51] L. A. Ostrovsky, A. M. Sutin, I. A. Soustova, A. L. Matveyev, A. I. Potapov and Z. Kluzek, "Nonlinear scattering of acoustic waves by natural and artificially generated subsurface bubble layers in sea," *J. Acoust. Soc. Am.,* vol. 113, no. 2, pp. 741-749, 2003.

[52] T. G. Leighton, D. G. Ramble and A. D. Phelps, "The detection of tethered and rising bubbles using multiple acoustic techniques," *Journal of the Acoustical Society of America,* vol. 101, no. 5, pp. 2626-2635, 1997.

[53] J. Tęgowski, J. Jakacki, Z. Klusek and S. Rudowski, “Nonlinear acoustical methods in the detection of gassy sediments in the Gulf of Gdansk”, *Hydroacoustics*, vol. 6, pp. 151–158, 2003.

[54] J. Tęgowski, Z. Klusek and J. Jakacki, “Nonlinear acoustical methods in the detection of gassy sediments”. In: A. Caiti, N. R. Chapman, J.P. Hermand, S. M. Jesus (Eds.) Acoustic Sensing Techniques for the Shallow Water Environment. Springer, Dordrecht. DOI: 10.1007/978-1-4020-4386-4_10

[55] A. L. Anderson and L. D. Hampton, "Acoustics of gas-bearing sediments I. Background," *J. Acoust. Soc. Am.,* vol. 67, no. 6, pp. 1865-1889, 1980.

[56] A. L. Anderson and L. D. Hampton, "Acoustics of gas-bearing sediment II. Measurements and models," *J. Acoust. Soc. Am.,* vol. 67, no. 6, pp. 1890-1903, 1980.

[57] F. A. Boyle and N. P. Chotiros, "A model for acoustic backscatter from muddy sediments," *J. Acoust. Soc. Am.,* vol. 98, pp. 525-530, 1995.

[58] G. Zheng, Y. Huang and J. Hua, "Sound speed, attenuation, and reflection in gassy sediments," *J. Acoust. Soc. Am.,* vol. 142, no. 2, pp. 530-539, 2017.

[59] Y. Wang, L. Huang, Y. L. Wang and P. Cheng, "Improved Anderson–Hampton acoustic velocity model for marine sandy gas-bearing sediments," in *IOP Conference Series: Materials Science and Engineering*, 2018.

[60] Z. Guangying and H. Xiumei, "The acoustic properties of gassy sediments due to gas-content fluctuations," in *10th International Conference on Wireless Communications and Signal Processing (WCSP)*, Hangzhou, 2018.

[61] H. Marin-Moreno, S. K. Sahoo and A. I. Best, "Theoretical modeling insights into elastic wave attenuation mechanisms in marine sediments with pore-filling methane hydrate," *Journal of Geophysical Research: Solid Earth,* vol. 122, no. 3, pp. 1835-1847, 2017.

[62] K. W. Commander and A. Prosperetti, "Linear pressure waves in bubbly liquids: Comparison between theory and experiments," *J. Acoust. Soc. Am.,* vol. 85, pp. 732-746, 1989.

[63] K. L. Williams, "An effective density fluid model for acoustic propagation in sediments derived from Biot theory," *The Journal of the Acoustical Society of America,* pp. 2276-2281, 2001.

[64] T. G. Leighton, The Acoustic Bubble, London: Academic Press, 1994.

[65] J. W. L. Clarke and T. G. Leighton, "A method for estimating time-dependent acoustic cross-sections of bubbles and bubble clouds prior to the steady state," *Journal of the Acoustical Society of America,* vol. 107, no. 4, pp. 1922-1929, 2000.

[66] See supplementary material at [*URL will be inserted by AIP*] for experiment locations on a map, exact execution times, and the ambient temperature and salinity values during each experiment. In this file (SuppPub1, with ReadMe in SuppPub5), the calibrated source amplitudes, and the pulse lengths for the transmission experiment, are also shown. Moreover, an example acoustic signal (transmitted by the transducer and recorded by the first two receivers of the line array) and the cross-correlation of its envelopes recorded by Receiver 1 and Receiver 2 are provided.

[67] G. Kan, D. Zou, B. Liu, J. Wang, X. Meng, G. Li and Y. Pei, “Correction for effects of temperature and pressure on sound speed in shallow seafloor sediments,” *Marine Georesources & Geotechnology*, vol. 37, no. 10, pp. 1217-1226, 2019.

[68] See supplementary material at [*URL will be inserted by AIP*] for the water tempeature (in SuppPub2, with ReadMe in SuppPub5) recorded in an area near to the experimental sites (Bramble Bank) (50.79219279836252, -1.2883804619098287) at 5-minute intervals on (a) 10 April 2009, (b)15 April 2009, (c) 10 June 2009, (d) 11 June 2009, (e) 22 July 2009, (f) 25 July 2009, (g) 28 July 2009, and (h) 04 August 2009. The column ‘WTMP’ in the data shows the water temperature recordings.

[69] A. Mantouka, T. G. Leighton, A. I. Best, J. K. Dix and P. R. White, "Inferring bubble populations in intertidal sediments from attenuation and scattering measurements," in

Proceedings of the Third International Conference on Underwater Acoustic Measurements, Technologies and Results, Nafplion, Greece, 2009, pp. 733-738.

[70] J. C. Lockwood and J. G. Willette, "High-speed method for computing the exact solution for the pressure variations in the nearfield of a baffled piston," *J. Acoust. Soc. Am.,* vol. 53, pp. 735-741, 1973.

[71] G. B. R. Robb, A. I. Best, J. K. Dix, P. R. White, T. G. Leighton, J. M. Bull and A. Harris, "Measurement of the in situ compressional wave properties in marine sediments," *IEEE Journal of Ocean Engineering,* vol. 32, no. 2, pp. 484-496, 2007.

[72] G. Robb, A. Best, J. Dix, J. Bull, T. Leighton and P. White, "The frequency dependence of compressional wave velocity and attenuation coefficient of intertidal marine sediments," *Journal of the Acoustical Society of America,* vol. 5, pp. 2526-2537, 2006.

[73] H. Cramer, Mathematical Methods of Statistics, Princeton: Princeton University Press, 1946, p. 575.

[74] C. H. Knapp and G. C. Carter, "The generalized correlation method for estimation of time delay," *IEEE Transactions on Acoustics, Speech, and Signal Processing*, vol. 24, pp. 320-327, 1976.

[75] T. Van Kessel and C. Blom, "Rheology of cohesive sediments: comparison between a natural and an artificial mud," *Journal of Hydraulic Research,* vol. 36, no. 4, pp. 591-612, 1998.

[76] Z. Huang and H. Aode, "A laboratory study of rhelogical properties of mudflows in Hangzhou Bay, China," *International Journal of Sediment Research,* vol. 24, no. 4, pp. 410-424, 2009.

[77] M. D. Richardson and K. B. Briggs, "In situ and laboratory geoacoustic measurements in soft mud and hard-packed sand sediments: Implications for high-frequency acoustic propagation and scattering," *Geo-Marine Letters,* vol. 16, pp. 196-203, 1996.

[78] S. M. Duffy, S. J. Wheeler and J. D. Bennell, "Shear modulus of kaolin containing methane bubbles," *J. Geotech. Eng.,* vol. 120, pp. 781-796, 1994.

[79] See supplementary material at [*URL will be inserted by AIP*] for the Transmission Experiment results (in SuppPub3, with ReadMe in SuppPub5), showing the group velocity and attenuation values at the Calshot site (a) on 10 April 2008, (c) on 10 June 2008 and (f) on 04 August 2008; and at the Mercury site (b, (c) on 15 April 2008 and (e) on 11 June 2008. In file (g), a statistical uncertainty analysis is provided that shows the mean and the standart deviation of the group velocity values, and the linear regression for the attenuation vs. frequency with the coefficient of determination (goodness-of-fit) values.

[80] E. L. Hamilton, "Compressional wave attenuation in marine sediments," *Geophysics,* vol. 4, pp. 620-646, 1972.

[81] E. G. McLeroy and A. DeLoach, "Sound speed and attenuation, from 15 to 1500 kHz, measured in natural seafloor sediments," *J. Acous. Soc. Am.,* vol. 44, pp. 1148-1150, 1968.

[82] S. S. Fu, R. H. Wilkens and L. N. Frazer, "In situ velocity profiles in gassy sediments: Kiel Bay," *Geo-Marine Letters,* vol. 16, pp. 249-253, 1996.

[83] See supplementary material at [*URL will be inserted by AIP*] for the Combination Frequency Experiment results (in SuppPub4, with ReadMe in SuppPub5), showing the received (scattered) pressure amplitudes (a) at the Calshot site on the 23 July 2008, and at the Mercury site (b) on 25 July 2008 and (c) 28 July 2008.

[84] M. S. Ballard and K. M. Lee, "The acoustics of marine sediments," *Acoustics Today,* vol. 3, pp. 11-18, 2017.

[85] E. I. Thorsos, K. L. Williams, N. P. Chotiros, J. T. Christoff, K. W. Commander, C. F. Greenlaw, D. V. Holliday, D. R. Jackson, J. L. Lopes, D. McGehee, J. E. Piper, M. D. Richardson and D. Tang, "An overviewof SAX99: Acoustic measurements," *IEEE Journal of Oceanic Engineering,* vol. 26, pp. 4-25, 2001.

[86] E. I. Thorsos, K. L. Williams, B. T. Hefner and D. R. Jackson, "Sediment sound speed and attenuation results from the sediment acoustics experiments in 1999 (SAX99) and 2004 (SAX04)," *J. Acoust. Soc. Am,* vol. 128, p. 2294, 2010.

[87] P. S. Wilson, D. P. Knobles and T. B. Neilsen, "Guest Editorial An Overview of the Seabed CharacterizationExperiment," *IEEE Journal of Oceanic Engineering,* vol. 1, pp. 1-13, 2020.

[88] M. Solan, C. Hauton, J. A. Godbold, C. L. Wood, T. G. Leighton and W. P., "Anthropogenic sources of underwater sound can modify how sediment-dwelling invertebrates mediate ecosystem properties," *Scientific Reports,* vol. 6, pp. 20540 (1-9), 2016.

[89] D. R. Jackson and M. D. Richardson, "Seasonal temperature gradients within a sandy seafloor: implications for acoustic propagation and scattering," in *Acoustical Oceanography: Proc. Inst. Acoustics.*, vol. 23, part 2, pp. 361-368 (Leighton, T.G., Heald, G.J., Griffiths, H. and Griffiths, G. eds., Bath University Press) Southampton, 9-12 April 2001.

[90] D. Zou, K. L. Williams and E. I. Thorsos, "Influence of temperature on acoustic sound speed and attenuation of seafloor sand sediment," *IEEE Journal of Oceanic Engineering,* vol. 40, pp. 969-980, 2015.

TABLES

TABLE 1: Geotechnical properties of the intertidal sites examined in this work: locations, sediment type, mean grain diameter, porosity and proportions of the constituent sediment types.

Location	Mean grain diameter(φ)	Porosity *n* (%)	Sand (%)	Silt (%)	Clay (%)	Organic content (%)
50° 48’56’’ N 001°18’4’’ W (Calshot)	6.0±0.5	62.0±5.0	27.5±7.0	69.7±6.5	2.8±0.4	3 ±0.5
50°52’56” N 001°18’34” W (Mercury marina)	6.7±0.2	60.0±2.5	7.6±5.0	82±3	9±3	9±0.5

FIGURE CAPTIONS

Figure 1: The gassy sediment experiment rig. R1, R2, R3 and R4 denote the locations of four hydrophone receivers which record the signals sent out from the pump source. The combination frequency apparatus consists of the high (imaging) frequency transmitter, the pump source and the high-frequency receiver. The imaging source and receiver have equal angular distances (45°) from the pump axis.

Figure 2: Photograph of the split core collected from (a) the Calshot site and (b) the Mercury site showing darker silt layers (a) and residual gas voids (b). Recalling the rig lay out (Fig. 1), the first, second and third hydrophones were buried at depths of approximately 21 cm, 35 cm and 50 cm, respectively. The dark grey color, as well as the hydrogen-sulphide odor, of the sediment core indicated that the measurements took place in the sulphate reduction zone.

Figure 3: (Color online) Equivalent plane wave group velocity and attenuation (i.e. the effects of geometrical spreading having been corrected out from these data) in gassy sediment in the frequency range 26 - 100 kHz as measured by the hydrophones 1 and 2 (unbroken black line) and hydrophones 2 and 3 (red dashed lines) at Calshot. The error bars indicate the standard deviation.

Figure 4: (Color online) Equivalent plane wave group velocity and attenuation in gassy sediment in the frequency range 26 - 100 kHz as measured by the hydrophones 1 and 2

(unbroken black line) and hydrophones 2 and 3 (red dashed lines) of the propagation rig at the Mercury site. The error bars indicate the standard deviation.

Figure 5: (Color online) (a) The received time signal for the 1-ms square wave insonification with f_p=44 kHz and f_i=220 kHz at the Calshot site on 23/07/2008, Measurement Set 6. In (b) the spectrogram of the same signal is shown where the two components of the dual frequency insonification are clearly observed.

Figure 6: Pressure amplitudes at the pump, difference and sum frequencies received at the location of the hydrophone. Data from the Hamble site on 25/07/2008 – measurement Set 1, plotted as a function of frequency. Error bars indicate the standard deviation obtained by the shots repeated.

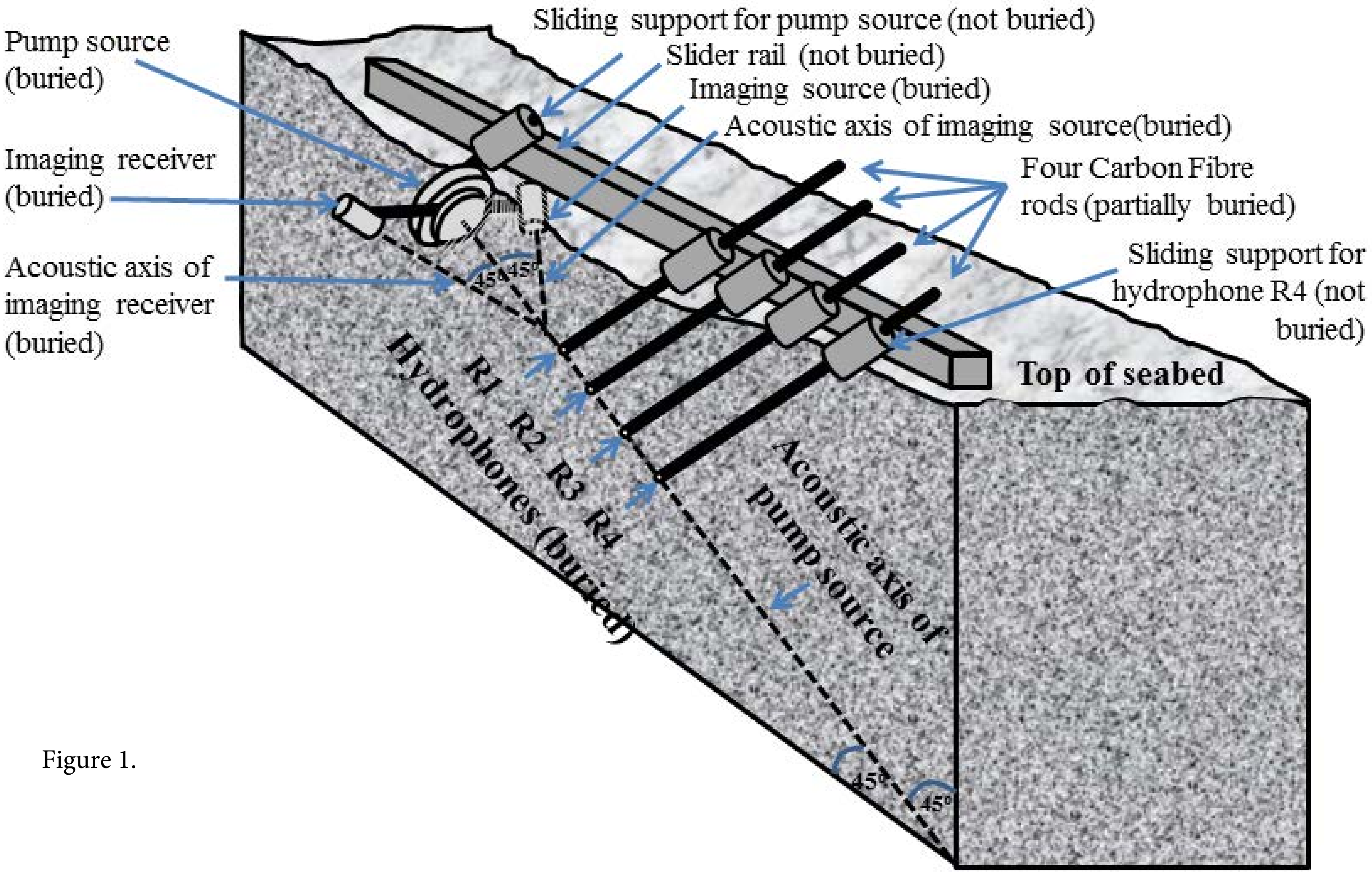
Sliding support for pump source (not buried)
Slider rail (not buried)
Imaging source (buried)
Acoustic axis of imaging source(buried)
Pump source (buried)
Imaging receiver (buried)
Four Carbon Fibre rods (partially buried)
Acoustic axis of imaging receiver (buried)
45°
45°
Sliding support for hydrophone R4 (not buried)
Top of seabed
R1
R2
R3
R4
Hydrophones (buried)
Acoustic axis of pump source
45°
45°

Figure 1.

Figure 2.

Figure 3.

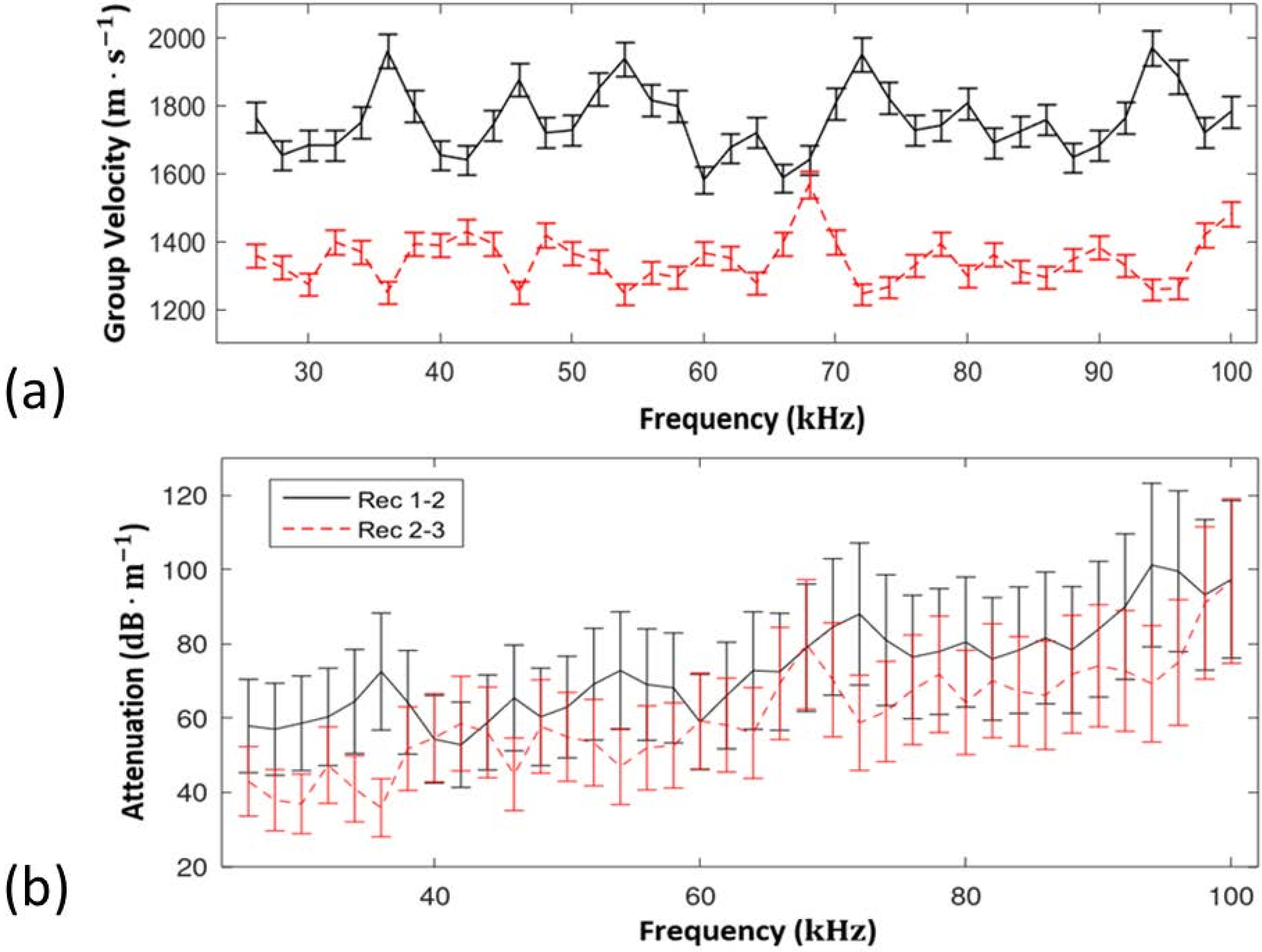
(a)
Group Velocity (m · s⁻¹)
2000
1800
1600
1400
1200
30
40
50
60
70
80
90
100
Frequency (kHz)
(b)
Attenuation (dB · m⁻¹)
120
100
80
60
40
20
40
60
80
100
Frequency (kHz)
Rec 1-2
Rec 2-3

Figure 4.

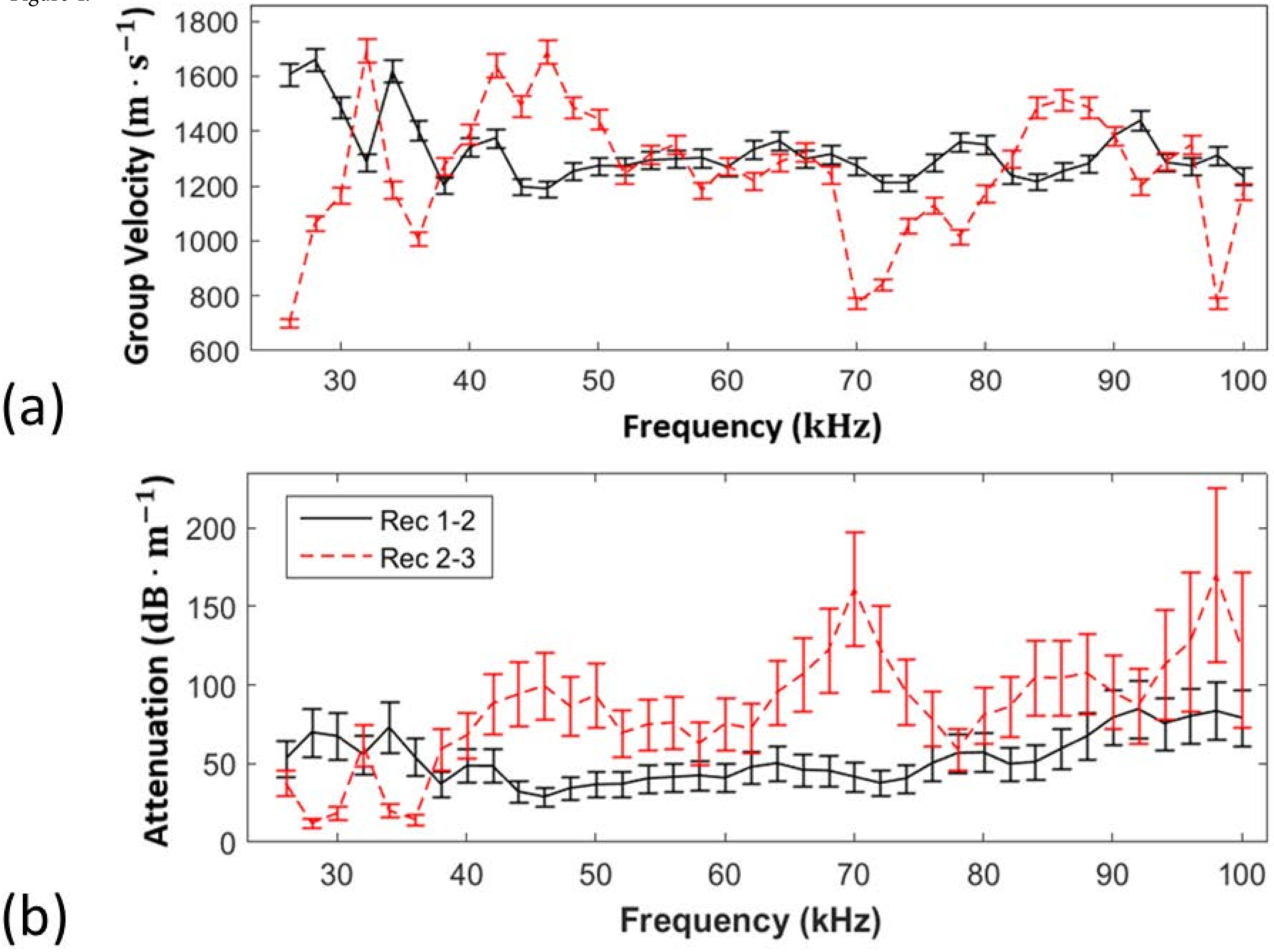
Group Velocity ($\mathrm{m \cdot s^{-1}}$)
1800
1600
1400
1200
1000
800
600
30
40
50
60
70
80
90
100
Frequency (kHz)
(a)
Attenuation ($\mathrm{dB \cdot m^{-1}}$)
200
150
100
50
0
Rec 1-2
Rec 2-3
30
40
50
60
70
80
90
100
Frequency (kHz)
(b)

Figure 5.

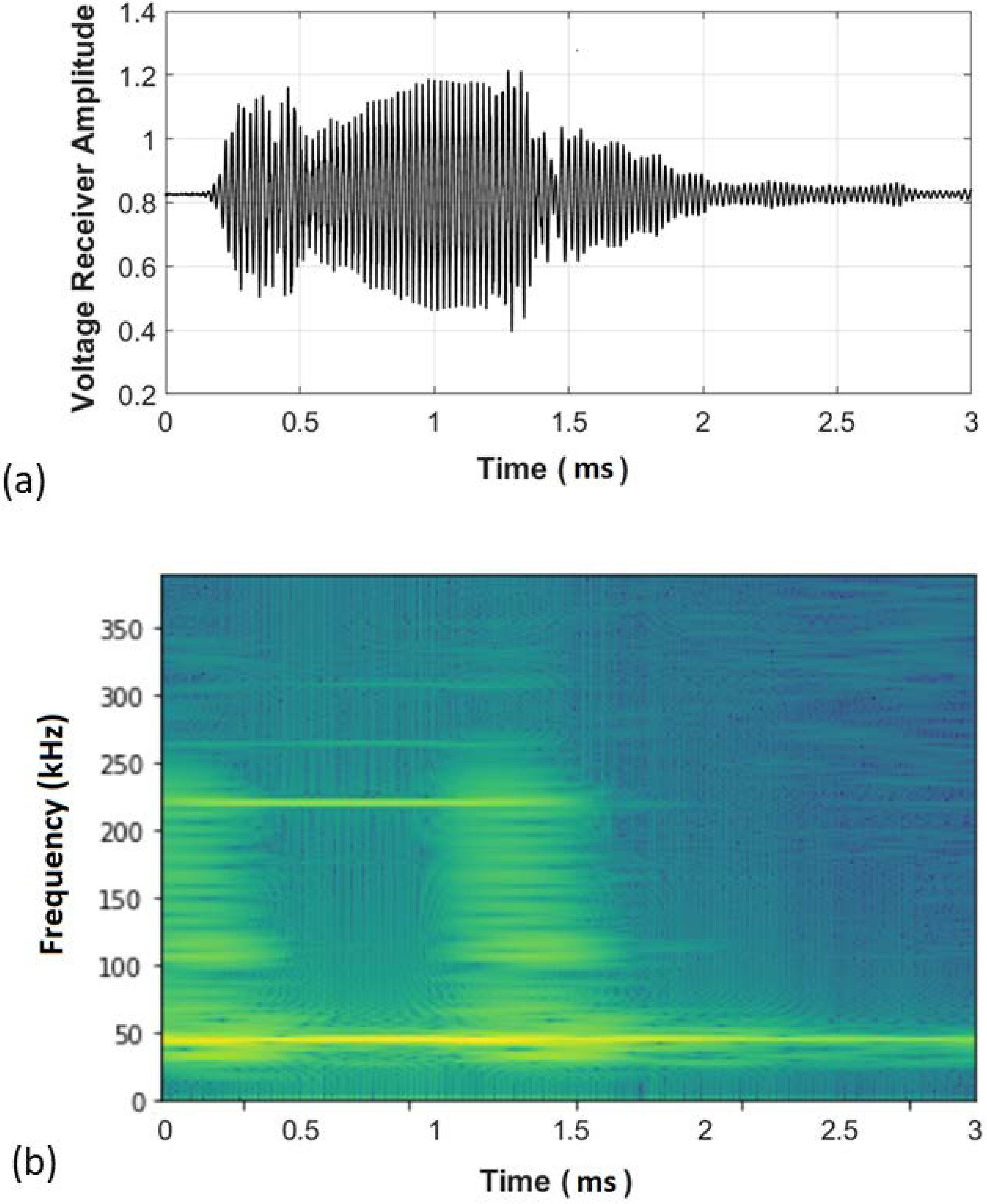
Voltage Receiver Amplitude
1.4
1.2
1
0.8
0.6
0.4
0.2
0
0.5
1
1.5
2
2.5
3
Time (ms)
(a)
Frequency (kHz)
350
300
250
200
150
100
50
0
0
0.5
1
1.5
2
2.5
3
Time (ms)
(b)

Figure 6.

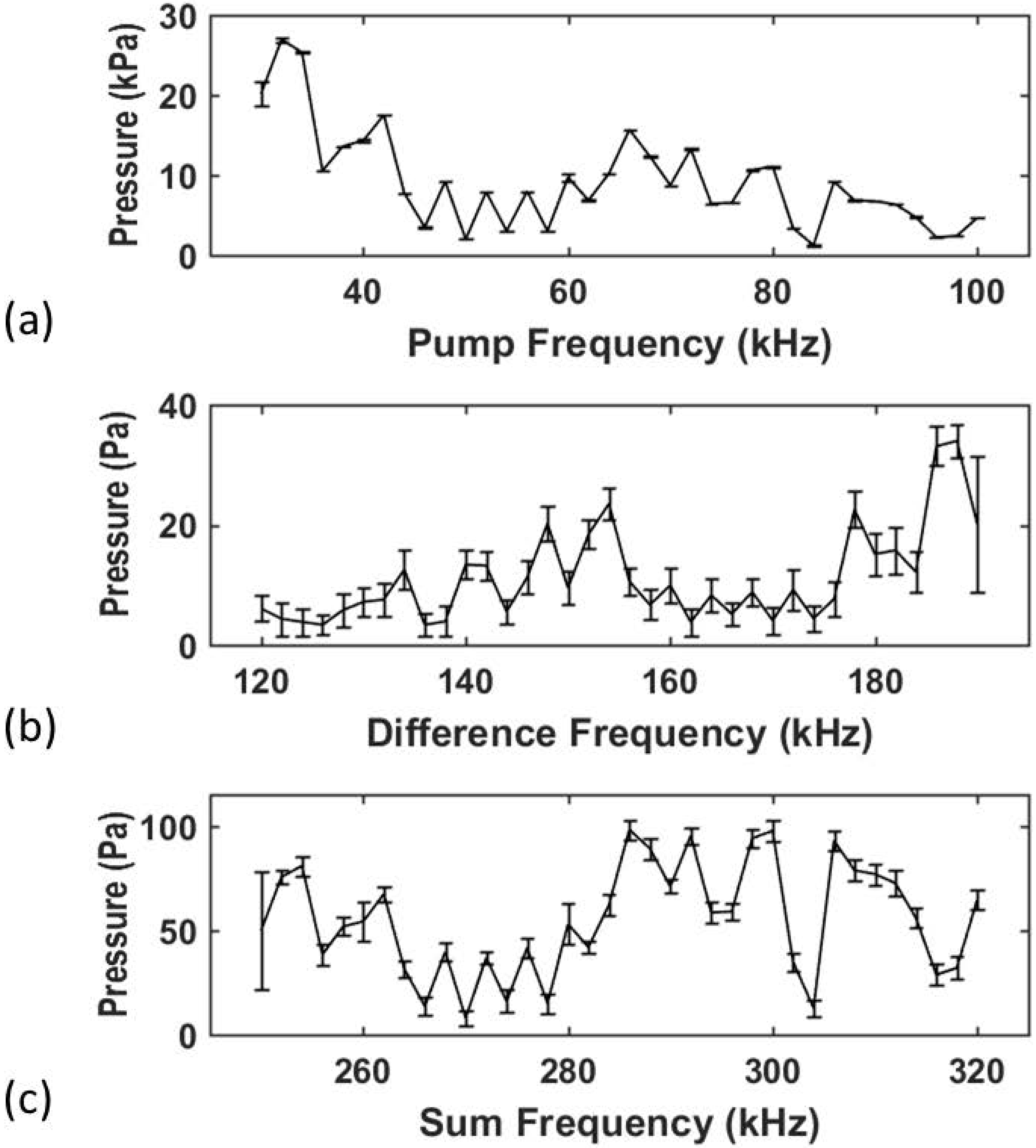

30
20
10
0
Pressure (kPa)
40
60
80
100
(a)
Pump Frequency (kHz)
40
20
0
Pressure (Pa)
120
140
160
180
(b)
Difference Frequency (kHz)
100
50
0
Pressure (Pa)
260
280
300
320
(c)
Sum Frequency (kHz)